Available online at www.sciencedirect.com
ScienceDirect
Journal of Power Sources 162 (2006) 823–828
JOURNAL OF POWER SOURCES
www.elsevier.com/locate/jpowsour

Short communication

Coating technique for improvement of the cycling stability of LiCo/NiO$_2$ electrode materials

E. Zhecheva [a,*], Ml Mladenov [b], R. Stoyanova [a], S. Vassilev [b]

[a] *Institute of General and Inorganic Chemistry, Bulgarian Academy of Sciences, 1113 Sofia, Bulgaria*
[b] *Institute of Electrochemistry and Energy Systems, Bulgarian Academy of Sciences, 1113 Sofia, Bulgaria*

Received 26 January 2005
Available online 13 September 2005

Abstract

We provide data on the changes in structure and composition of commercial $LiNi_{0.8}Co_{0.2}O_2$ electrode materials for lithium-ion batteries occurring after surface coating with two types of metal oxides: electrochemically active $LiCoO_2$ and inactive MgO. XRD analysis, SEM images, IR spectroscopy and EPR of low-spin Ni^{3+} ions were carried out for structural characterisation of coated $LiNi_{0.8}Co_{0.2}O_2$ electrodes. Surface modification with $LiCoO_2$ was found to be a more effective route for improving the cycling stability of $LiNi_{0.8}Co_{0.2}O_2$. The favourable effect of $LiCoO_2$-coating was connected with an enhanced stability of the bulk composition and reduction of electrode/electrolyte interaction.

Keywords: Coating technique; Cathode materials; Structural characterisation; Lithium ion batteries; Cycling stability

1. Introduction

The coating technique has recently been considered as an alternative method for improvement of the electrochemical performance of electrode materials for lithium-ion batteries [1–10]. This method consists in surface treatment of electrode materials with metal oxides (MgO, Al_2O_3, SnO_2, TiO_2, ZrO_2, SiO_x, $AlPO_4$, etc.) which do not participate in the electrochemical reaction. It has been shown that coated electrodes display a higher capacity retention during prolonged cycling in the extended potential range at elevated temperatures. However, it is still unclear whether a better bulk or/and surface stability contribute to the capacity retention of coated electrodes. In addition, it has been reported that an improvement of the capacity retention of commercial $LiCoO_2$-based electrodes can be achieved merely by controlled heat-treatment (up to 550 °C) [11]. Another approach to the improvement of the electrode performance is based on the deposition of an electrochemically active oxide (such as $LiMn_2O_4$ spinel) on the electrode surface [12,13]. These results highlight the important role of the surface state of the electrode materials with respect to their electrochemical performance.

The surface interaction of commercial $LiNi_{0.8}Co_{0.2}O_2$ cathode materials with $Mg(CH_3COO)_2$ at 600 °C has been studied in details in previous studies of us [14]. It has been found that the bulk composition remains free from Mg-dopants, but two kinds of Mg-phases are formed on the $LiNi_{0.8}Co_{0.2}O_2$ surface: a thin layer of a "xMgO·$(1-x)$$LiNi_{0.8}Co_{0.2}O_2$" solid solution ($x<0.2$) and MgO-like deposits. While the surface solid solution "xMgO·$(1-x)$$LiNi_{0.8}Co_{0.2}O_2$" reacts electrochemically with Li, the MgO-deposits are electrochemically inactive. As a result, the best electrochemical performance is observed for samples having a surface coating of a "xMgO·$(1-x)$$LiNi_{0.8}Co_{0.2}O_2$" phase with a high Mg-content and minimum MgO deposits on the particle surface.

In this paper we provide data on the changes in structure and composition of commercial $LiNi_{0.8}Co_{0.2}O_2$ electrode materials occurring after surface coating with the electrochemically active $LiCoO_2$. This oxide was chosen due to

* Corresponding author. Tel.: +359 2 979 3915; fax: +359 2 870 5024.
E-mail address: zhecheva@svr.igic.bas.bg (E. Zhecheva).

0378-7753/$ – see front matter © 2005 Elsevier B.V. All rights reserved.
doi:10.1016/j.jpowsour.2005.07.063

its ability to form solid solutions with $LiNiO_2$. For the sake of comparison, a commercial $LiNi_{0.8}Co_{0.2}O_2$ electrode was coated with inactive MgO. Structural characterisation of coated $LiNiCoO_2$ electrodes was performed by XRD diffraction, scanning electron microscopy, IR spectroscopy and electron paramagnetic resonance spectroscopy (EPR) of Ni^{3+} ions. The electrochemical performance of uncoated and coated electrodes was evaluated in constant current experiments at 25 and 55 °C. The plausible "electrolyte–electrode" reaction was followed by IR spectroscopy, while ex situ XRD and EPR of Ni^{3+} were used to probe bulk electrode composition.

2. Experimental

Commercially available cathode powder of $LiNi_{0.8}Co_{0.2}O_2$ from MERCK was used as pristine material. The initial samples (2 g) were immersed in ethanolic solution of $Li(CH_3COO)\cdot 4H_2O$ and $Co(CH_3COO)_2\cdot 4H_2O$ or $Mg(CH_3COO)_2\cdot 4H_2O$ (0.02 M), followed by ethanol evaporation at 30 °C under atmospheric pressure. The Mg to (Ni + Co) and (Li + Co) to (Ni + Co) ratios were 0.02. The solid residue thus obtained was heated at 600 °C under oxygen. The lithium and Mg contents of the samples and the mean oxidation state of nickel and cobalt were determined by atomic absorption analysis and iodometric titration, respectively.

The X-ray phase analysis was performed with a Philips diffractometer, using Cu Kα-radiation and a graphite monochromator. The unit cell parameters were obtained by least-squares fitting of all peak positions ($15 \leq 2\Theta \leq 90$). IR spectra were recorded on a NICOLET AVATAR-320 spectrometer in KBr pellets. Scanning electron microscopy (SEM) measurements were carried out on a Jeol-100 B microscope with 120 kV acceleration voltage. The SEM observations were made on samples coated with an Au-conducting layer as well as on uncoated samples. The EPR spectra were registered as the first derivative of the absorption signal using an ERS-220/Q spectrometer (ex-GDR) within the temperature range 90–400 K. The *g*-factors were established with respect to a Mn^{2+}/ZnS standard.

The samples were cycled as cathodes in special laboratory stainless steel cells with a steel spring in order to maintain a definite pressure upon the electrode face. The anodes in the cell were Li metal discs. The electrolyte was 1 M $LiClO_4$ solution in EC + PC (1:1, v/v) with less than 20 ppm of water. The electrodes were separated by glass fibber paper (Amer-Sill). The samples were mixed with teflonized acetylene black (TAB-2) in a 80:20 weight ratio. The 15 mm disc cathodes were prepared by pressing the cathode mixture on Al foil discs. The cells were charged and discharged at a constant current of 30 mA g^{-1} of the active material (~0.5 mA cm^{-2}) in the voltage range of 4.3–3.0 and 4.2–3.0 V at 25 and 55 °C.

3. Results and discussion

3.1. Structural characterisation of $LiCoO_2$-coated $LiNi_{0.8}Co_{0.2}O_2$

It has already been reported that thermal decomposition of lithium–cobalt acetates at 600 °C yields $LiCoO_2$ with a pseudo-spinel structure [15]. However, surface treatment of $LiNi_{0.8}Co_{0.2}O_2$ with a $Li(CH_3COO)$–$Co(CH_3COO)_2$ mixture at 600 °C has no effect on the XRD pattern. XRD patterns of treated $LiNi_{0.8}Co_{0.2}O_2$ have been indexed in the *R*-3*m* space group with unit cell dimensions similar to those of untreated $LiNi_{0.8}Co_{0.2}O_2$ (Table 1). The same result was obtained with $LiNi_{0.8}Co_{0.2}O_2$ coated with MgO (Table 1).

The SEM images of uncoated and coated oxides also remain the same after surface treatment. Well-crystallised particles with dimensions between 400 and 1000 nm can be distinguished. This result is consistent with SEM analysis of MERCK available $LiNi_{0.8}Co_{0.2}O_2$ cathode materials [10,14].

To analyse the surface composition of Li–Co-treated $LiNi_{0.8}Co_{0.2}O_2$, EPR spectroscopy of low-spin Ni^{3+} was undertaken. Our previous EPR studies on $LiNi_{1-x}Co_xO_2$ solid solutions showed that EPR spectroscopy was a suitable experimental tool to assess the local environment of Ni^{3+} in respect of diamagnetic Co^{3+} and paramagnetic Ni^{3+} ions [16]. This information can be extracted from the analysis of the EPR line width: the line width increases with the Ni content, going through a maximum at Ni/(Co + Ni) = 0.67 [16]. The dependence of the line width on the Ni content is a consequence of the development of both magnetic dipole–dipole and exchange interactions.

Fig. 1 gives the EPR spectra of bare and coated $LiNi_{0.8}Co_{0.2}O_2$. Between 100 and 300 K, both EPR spectra consist of a main Lorentzian line with $g = 2.137$ and a line width of about 200 mT. The EPR parameters of this signal correspond to exchange coupled Ni^{3+} ions. The preservation

Table 1
Unit cell parameters (*a* and *c*) of pristine $LiNi_{0.8}Co_{0.2}O_2$ and electrodes after 30 cycles between 3.0 and 4.3 V at 25 and 55 °C: bare $LiNi_{0.8}Co_{0.2}O_2$, MgO-coated $LiNi_{0.8}Co_{0.2}O_2$, and $LiCoO_2$-coated $LiNi_{0.8}Co_{0.2}O_2$

Samples	*a* (Å) (±0.0004)			*c* (Å) (±0.0016)		
	Pristine	25 °C	55 °C	Pristine	25 °C	55 °C
$LiNi_{0.8}Co_{0.2}O_2$	2.8681	2.8674	2.8539	14.1576	14.2697	14.2894
MgO–$LiNCoO_2$	2.8677	2.8634	2.8628	14.1591	14.2328	14.2406
$LiCoO_2$–$LiNiCoO_2$	2.8675	2.8545	2.8593	14.1584	14.2456	14.2347

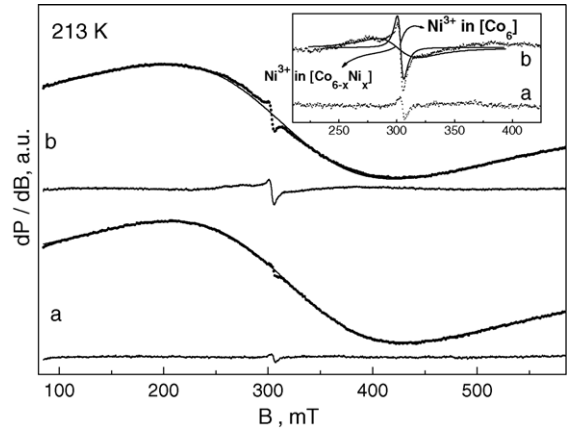

Fig. 1. EPR spectra of bare $LiNi_{0.8}Co_{0.2}O_2$ (a) and $LiCoO_2$-coated $LiNi_{0.8}Co_{0.2}O_2$ (b). The difference between experimental and simulated spectra is shown. The inset gives the simulated EPR signals corresponding to Ni^{3+} ions in nearly pure $LiCoO_2$ (Ni^{3+} in [Co_6]) and $LiNi_{\sim 0.1}Co_{\sim 0.9}O_2$ (Ni^{3+} in [$Co_{6-x}Ni_x$]).

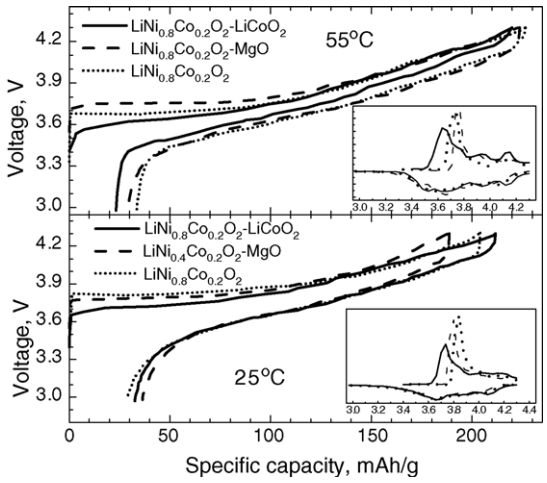

Fig. 2. Charge/discharge curves at 25 and 55 °C for bare $LiNi_{0.8}Co_{0.2}O_2$ (dotted line), MgO-coated $LiNi_{0.8}Co_{0.2}O_2$ (dashed line) and $LiCoO_2$-coated $LiNi_{0.8}Co_{0.2}O_2$ (full line). Inset shows the first derivatives of the charge/discharge curves.

of the EPR parameters after coating gives evidence that the bulk composition of $LiNi_{0.8}Co_{0.8}O_2$ remains unchanged.

Close inspection of the EPR spectra of bare and coated oxides reveals two narrow low-intensity signals in the range of $2.12 < g < 2.18$ (Fig. 1). The first signal with $g = 2.14$ and a line width of 5.6 mT is visible in the EPR spectrum of bare and treated samples. However, the intensity of this signal increases after the treatment of $LiNi_{0.8}Co_{0.2}O_2$ with lithium cobaltate. The second low-intensity signal, having $g = 2.15$ and a line width of 35 mT, is detected in the EPR spectrum of Li–Co-treated $LiNi_{0.8}Co_{0.2}O_2$ only. Taking into account the dependence of the EPR line width of Ni^{3+} on the Ni/Co-ratio, these parameters allow assigning the two low-intensity signals to Ni^{3+} having different numbers of diamagnetic Co^{3+} and paramagnetic Ni^{3+} neighbours. In order to analyse the surface composition, the EPR line width of Ni^{3+} in Co-substituted $LiNiO_2$ was determined. For $LiNi_{1-x}Co_xO_2$ with $x = 0.8$, 0.9 and 0.99, the line width was 90, 40 and 6 mT, respectively. Comparison showed that the EPR line widths of two low-intensity signals detected on Li–Co-treated $LiNi_{0.8}Co_{0.2}O_2$ were close to that for Ni^{3+} in nearly pure lithium cobaltate and slightly Ni-substituted $LiCoO_2$ ($LiNi_{0.01}Co_{0.99}O_2$ and $LiNi_{\sim 0.1}Co_{\sim 0.9}O_2$, respectively).

This result indicates that the treatment of $LiNi_{0.8}Co_{0.2}O_2$ with a Li–Co-acetate mixture at 600 °C proceeds via the formation of Co-rich oxides with a composition close to nearly pure $LiCo_{0.99}O_2$ and Ni-doped $LiCoO_2$ ($LiNi_{\sim 0.1}Co_{\sim 0.9}O_2$) without affecting the bulk composition of $LiNi_{0.8}Co_{0.2}O_2$. However, the EPR studies do not permit establishing the location of the Co-rich phases in the $LiNi_{0.8}Co_{0.2}O_2$ particles. Considering the ability of $LiNiO_2$ to form solid solutions with $LiCoO_2$, we can suggest that nearly pure $LiCoO_2$ is on the top surface of $LiNi_{0.8}Co_{0.2}O_2$ particles, while the Ni-doped $LiCoO_2$ phase ensures the contacts between $LiNi_{0.8}Co_{0.2}O_2$ and surface lithium cobaltate. A similar picture has been established after surface interaction of magnesium acetate with $LiNi_{0.8}Co_{0.2}O_2$ at 600 °C, where Mg is distributed between "xMgO·$(1-x)$$LiNi_{0.8}Co_{0.2}O_2$" surface solid solution and MgO-deposits [14].

3.2. *Effect of the $LiCoO_2$-coating on the electrochemical performance of $LiNi_{0.8}Co_{0.2}O_2$*

The coated compositions were tested as electrode materials in lithium ion cells in constant current experiments at 25 and 55 °C. Fig. 2 compares the first charge/discharge curves of bare and coated oxides. As one can see, the kinetic limitations at both 25 and 55 °C are drastically reduced after the treatment of $LiNi_{0.8}Co_{0.2}O_2$ with $LiCoO_2$. As a result, the first discharge capacity is higher for $LiCoO_2$-treated $LiNi_{0.8}Co_{0.2}O_2$. At 25 °C, the interfacial resistance of the MgO-treated electrode is higher and can be associated with the surface deposits of inactive MgO. At 55 °C, the interfacial resistances for bare and MgO-treated oxides become nearly the same.

To outline the effect of the coating on the cycling stability, Table 2 presents of comparison of the capacity efficiency of bare and coated electrodes. It is important that the coating affects more significantly the electrochemical performance at elevated temperatures. The effect of coating becomes noticeable at 55 °C after five cycles of lithium extraction/insertion, while at 25 °C the coated oxides display a higher capacity efficiency after the 30th cycle. The increased capacity retention for coated oxides is observed for both potential ranges used: 4.3–3.0 and 4.2–3.0 V. With increasing the rate of lithium extraction/insertion, the first discharge capacities decrease and, after the 15th cycle, the coated oxides deliver a higher capacity as compared to the bare oxide. The better capacity retention with MgO- and $LiCoO_2$-coated $LiNi_{0.8}Co_{0.2}O_2$ is consistent with the data on the improved electrochemical

Table 2
First discharge capacity and capacity efficiency for bare $LiNi_{0.8}Co_{0.2}O_2$, MgO-coated $LiNi_{0.8}Co_{0.2}O_2$, and $LiCoO_2$-coated $LiNi_{0.8}Co_{0.2}O_2$ electrodes cycled between 4.2–3.0 and 4.3–3.0 V at 25 and 55 °C

Samples	4.3–3.0 V, *C*/10				4.2–3.0 V, *C*/10				4.2–3.0 V, *C*/3			
	25 °C		55 °C		25 °C		55 °C		55 °C			
	First discharge capacity ($mAh\,g^{-1}$)	Capacity efficiency (30 cycles) (%)	First discharge capacity ($mAh\,g^{-1}$)	Capacity efficiency (5 cycles)	First discharge capacity ($mAh\,g^{-1}$)	Capacity efficiency (30 cycles) (%)	First discharge capacity ($mAh\,g^{-1}$)	Capacity efficiency (15 cycles) (%)	First discharge capacity ($mAh\,g^{-1}$)	Capacity efficiency (15 cycles) (%)		
$LiNi_{0.8}Co_{0.2}O_2$	175	78	193	79	158	87	179	78	150	82		
MgO–$LiNiCoO_2$	155	92	195	88	150	90	178	85	155	92		
$LiCoO_2$–$LiNiCoO_2$	179	87	197	94	168	92	190	85	172	89		

performance of layered $LiMO_2$ coated with electrochemically inactive metal oxides [1–9]. An important feature of our finding is the differentiation between the electrochemical performances of $LiNi_{0.8}Co_{0.2}O_2$ electrodes coated with inactive MgO and active $LiCoO_2$. Comparison shows a better electrochemical performance of $LiNi_{0.8}Co_{0.2}O_2$ coated with $LiCoO_2$, especially at elevated temperature and higher cycling rate.

It is well recognised that the cycling stability of layered $LiMO_2$ electrodes is a complex phenomenon determined by both interface and bulk instability. Ex situ XRD analysis, IR spectroscopy and EPR of Ni^{3+} on cycled electrodes were carried out in order to analyse the observed cycling stability of coated oxides. Discharged samples after 30 cycles between 4.3–3.0 V at 25 and 55 °C were analysed. Under these conditions, the XRD patterns of bare and coated electrodes reveal that the layered crystal structure is preserved, the unit cell dimensions being given in Table 1. There are strong changes in the unit cell dimensions due to the unrecovered compositions. The changes are more significant for bare $LiNi_{0.8}Co_{0.2}O_2$ cycled at 55 °C. An important feature of the XRD patterns is the selective broadening of the (1 1 0) diffraction line observed only for bare $LiNi_{0.8}Co_{0.2}O_2$ when it is cycled at 55 °C (Fig. 3). The broadening of the (1 1 0)

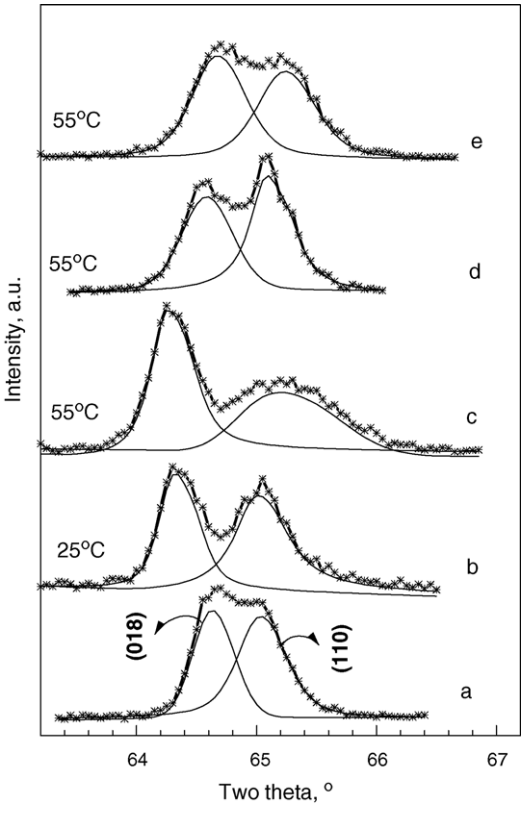

Fig. 3. XRD (1 0 8) and (1 1 0) diffraction peaks for pristine $LiNi_{0.8}Co_{0.2}O_2$ (a), $LiNi_{0.8}Co_{0.2}O_2$ electrode after 30 cycles at 25 °C (b), $LiNi_{0.8}Co_{0.2}O_2$ electrode after 30 cycles at 55 °C (c), MgO-coated $LiNi_{0.8}Co_{0.2}O_2$ electrode after 30 cycles at 55 °C (d) and $LiCoO_2$-coated $LiNi_{0.8}Co_{0.2}O_2$ electrode after 30 cycles at 55 °C (e).

diffraction line points to the formation of extended defects in the main (1 1 0) plane of $LiNi_{0.8}Co_{0.2}O_2$ caused by Li extraction/insertion at 55 °C. This feature is not observed with MgO- and $LiCoO_2$-coated electrodes, which indicates that the coating layer prevents the bulk $LiNi_{0.8}Co_{0.2}O_2$ compositions from the formation of extended defects.

Ex situ EPR of Ni^{3+} ions has been used to obtain further information on changes occurring during Li extraction/insertion at 55 °C. The EPR spectra of cycled compositions consist of a single Lorentzian line due to exchange coupled Ni^{3+} ions. For all the cycled compositions at 25 °C, the line width is higher as compared to that of the uncycled compositions: the line width determined at 103 K is 202, 183 and 195 mT for bare $LiNi_{0.8}Co_{0.2}O_2$, MgO-coated $LiNi_{0.8}Co_{0.2}O_2$ and $LiCoO_2$-coated $LiNi_{0.8}Co_{0.2}O_2$, respectively, versus 218, 215 and 220 mT for the corresponding cycled compositions (Fig. 4). This broadening can be explained by the appearance of diamagnetic Ni^{4+} ions in the unrecovered composition of the electrodes after several cycles of Li extraction/insertion. Contrary to electrodes cycled at room temperature, the line width of Ni^{3+} for all electrodes cycled at 55 °C decreases (Fig. 4): 155, 161 and 177 mT for bare $LiNi_{0.8}Co_{0.2}O_2$, MgO-coated $LiNi_{0.8}Co_{0.2}O_2$ and $LiCoO_2$-coated $LiNi_{0.8}Co_{0.2}O_2$, respectively. Based on the relationship between the EPR line width and the Ni/Co ratio in $LiNi_{1-x}Co_xO_2$ [16], the lower EPR line width clearly demonstrates changes in the bulk Ni/Co ratio due to bulk instability during electrochemical reaction at elevated temperatures (55 °C). However, the changes in the bulk Ni/Co ratio proceed via the preservation of the layered crystal structure. Based on atomic force microscopy and Raman microscopy, it has been found that the high-temperature capacity loss with $LiNi_{0.8}Co_{0.2}O_2$ is a result of the surface phase degradation into Co and Ni oxides [17]. The EPR results show that changes in the Ni/Co ratio comprise deeper layers. In addition, the slightly broader EPR signal detected for cycled coated oxides as compared

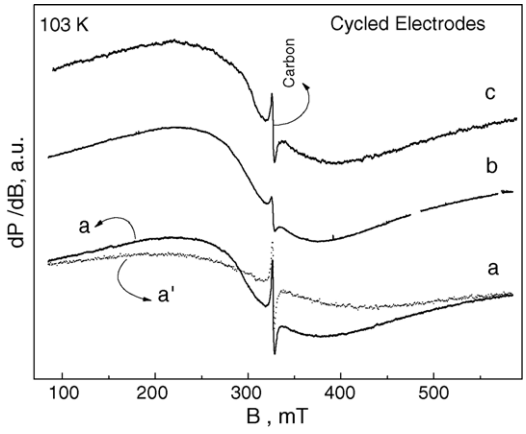

Fig. 4. EPR spectra at 103 K of bare $LiNi_{0.8}Co_{0.2}O_2$ (a), MgO-coated $LiNi_{0.8}Co_{0.2}O_2$ (b) and $LiCoO_2$-coated $LiNi_{0.8}Co_{0.2}O_2$ (c) electrodes after the 30th discharge up to 3.0 V at 55 °C. For the sake of comparison, curves (a′) corresponds to a bare $LiNi_{0.8}Co_{0.2}O_2$ electrode cycled at 25 °C.

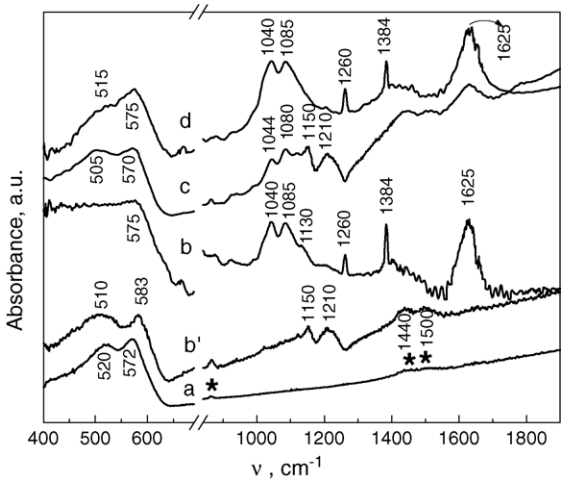

Fig. 5. IR spectra of pristine $LiNi_{0.8}Co_{0.2}O_2$ (a), $LiNi_{0.8}Co_{0.2}O_2$ electrode after 30th discharge up to 3.0 V at 25 °C (b′) and 55 °C (b), MgO-coated $LiNi_{0.8}Co_{0.2}O_2$ electrode cycled at 55 °C (c), and $LiCoO_2$-coated $LiNi_{0.8}Co_{0.2}O_2$ electrode cycled at 55 °C (d). The vibrations due to the CO_3^{2-}-group are denoted with asterisk (*).

to cycled bare oxide indicates that the bulk instability of the $LiNi_{0.8}Co_{0.2}O_2$ electrode is suppressed by the coating, especially by the $LiCoO_2$-coating. Another important feature of the EPR spectrum of the $LiCoO_2$-coated oxide is the disappearance of the two narrow low-intensity signals of Ni^{3+} ions in a Co^{3+}-rich environment.

The plausible interface electrolyte–electrode interaction has been thought to be one of the reasons for the observed capacity fade with $LiNi_{0.8}Co_{0.2}O_2$ [18–20]. To understand this behaviour, we have performed FTIR analysis of bare and coated $LiNi_{0.8}Co_{0.2}O_2$ electrodes after the 30th cycle at 55 °C (Fig. 5). Two regions can be outlined in the IR spectra: the first one between 400 and 800 cm^{-1}, where Ni/CoO_2-vibrations are observed [21,22], and the second between 1000 and 1700 cm^{-1}, where the vibrations of functional organic groups appear [18,23,24]. While the IR region between 400 and 800 cm^{-1} provides information on the structural changes in the bulk of $LiNi_{0.8}Co_{0.2}O_2$, the second IR region (above 1000 cm^{-1}) reveals the interaction of $LiNi_{0.8}Co_{0.2}O_2$ with the electrolyte. In accordance with the XRD and EPR data, the IR modes due to Ni/CoO_2-vibrations are changed in terms in positions and band intensity distribution, the changes being more significant for the bare $LiNi_{0.8}Co_{0.2}O_2$ electrode. When the cell is cycled at room temperature, there are smooth changes in peak positions of the two IR modes in the 400–800 cm^{-1} range, their intensity being not affected. This picture is seen with both bare and coated electrodes. The IR results confirm the finding derived from XRD and EPR on the changes in the Ni/Co bulk compositions during the electrochemical reaction at elevated temperatures only. In addition, the limited changes in the IR modes of Ni/CoO_2-vibrations with $LiCoO_2$-coated $LiNi_{0.8}Co_{0.2}O_2$ outline once again the bulk stabilizing effect of the $LiCoO_2$ coating.

Above 1000 cm^{-1}, the IR spectra of bare and coated $LiNi_{0.8}Co_{0.2}O_2$ electrodes display diffuse peaks in the range of 1400–1500 cm^{-1}. According to the IR data on layered $LiMO_2$ oxides [19,21], these peaks correspond to a carbonate group of Li_2CO_3, which remains usually on the surface of pristine oxides during the synthesis. When bare and coated electrodes are cycled at room temperature, the peaks due to Li_2CO_3 do not disappear (Fig. 5). This means that impurity Li_2CO_3 is maintained after electrochemical reaction at room temperature. In addition, new peaks at 1150 and 1210 cm^{-1} are observed. According to the IR study on the electrolyte solutions, these new peaks can be attributed to O–C–O stretching vibration of the PC ring [18,23]. Since the most intense IR mode for PC at 1790 cm^{-1} corresponding to C=O stretching vibration [18,23] is not observed for the cycled samples, this result demonstrates oxidation of the electrolyte on bare and coated $LiNi_{0.8}Co_{0.2}O_2$ electrodes rather than occluded or adsorbed solvent on electrode materials after cycling. When bare and coated oxides are cycled at high temperatures, there is a drastic change in the IR spectra above 1000 cm^{-1}. New peaks at 1625, 1384, 1260, 1130, 1085 and 1040 cm^{-1} become recognizable. The peaks at 1625, 1450–1350 and 1130 cm^{-1} can be assigned to functional groups of $ROCO_2Li$, while the additional peaks in the range of 1000–1100 cm^{-1} can be related to the stretching vibrations of the C–O bond coming from EC. This result shows the formation of a passivating layer consisting of $ROCO_2Li$ and oxidation products of EC after the electrochemical reaction at 55 °C. While the IR profile of MgO-coated $LiNi_{0.8}Co_{0.2}O_2$ electrodes cycled at 55 °C is similar to that of the bare $LiNi_{0.8}Co_{0.2}O_2$ electrode, the IR spectrum of the $LiCoO_2$-coated $LiNi_{0.8}Co_{0.2}O_2$ electrode cycled at 55 °C is a superposition of the IR spectra of bare $LiNi_{0.8}Co_{0.2}O_2$ electrodes cycled at 25 and 55 °C. This result clearly shows that the $LiCoO_2$-coating impedes the reaction between the electrolyte and the electrode surface.

4. Conclusions

The treatment of $LiNi_{0.8}Co_{0.2}O_2$ with a Li–Co-acetate mixture at 600 °C proceeds via surface formation of Co-rich oxides with compositions close to nearly pure $LiCoO_2$ ($LiNi_{0.01}Co_{0.99}O_2$) and Ni-doped $LiCoO_2$ ($LiNi_{\sim 0.1}Co_{\sim 0.9}O_2$), the bulk composition of $LiNi_{0.8}Co_{0.2}O_2$ being not affected. The coated electrode displays an improved capacity retention at both elevated temperatures and high cycling rates. The favourable effect of the $LiCoO_2$-coating can be related to the enhanced stability of the bulk composition, as well as to the suppression of the reaction between the electrode surface and the electrolyte.

Acknowledgements

The authors acknowledge financial support from the National Science Fund of Bulgaria (Contract No. Ch1304/2003). The authors are grateful to MERCK KGa for the donation of the cathode materials.

References

[1] H.-J. Kweon, D.G. Park, Electrochem. Solid-State Lett. 3 (2000) 128.
[2] H.-J. Kweon, S.J. Kim, D.G. Park, J. Power Sources 88 (2000) 255.
[3] J. Cho, Y.J. Kim, Y.J.B. Park, Chem. Mater. 12 (2000) 3788.
[4] J. Cho, C.-S. Kim, S.-I. Yoo, Electrochem. Solid-State Lett. 3 (2000) 362.
[5] M. Mladenov, R. Stoyanova, E. Zhecheva, S. Vassilev, Electrochem. Commun. 3 (2001) 410.
[6] J. Cho, Y.J. Kim, B. Park, J. Electrochem. Soc. 148 (2001) A1110.
[7] A. Choblet, H.C. Shiao, H.-P. Lin, M. Salomon, V. Manivannan, Electrochem. Solid-State Lett. 4 (2001) A65.
[8] Zh. Wang, Ch. Wu, L. Liu, F. Wu, L. Chen, X. Huang, J. Electrochem. Soc. 149 (2002) A466.
[9] L. Liu, L. Chen, X. Huang, X.-Q. Yang, W.-S. Yoon, H.S. Lee, J. McBreen, J. Electrochem. Soc. 151 (2004) A1344.
[10] H. Omada, T. Brouse, C. Marhic, D.M. Schleich, J. Electrochem. Soc. 151 (2004) A922.
[11] Zh. Chen Chen, J.R. Dahn, Electrochem. Solid-State Lett. 7 (2004) A11.
[12] J. Cho, G. Kim, Electrochem. Solid State Lett. 2 (1999) 253.
[13] J. Cho, Solid State Ionics 160 (2003) 241.
[14] E. Zhecheva, R. Stoyanova, G. Tyuliev, K. Tenchev, M. Mladenov, S. Vassilev, Solid State Sci. 5 (2003) 711.
[15] E. Zhecheva, R. Stoyanova, M. Gorova, R. Alcantara, J. Morales, J.-L. Tirado, Chem. Mater. 8 (1996) 1429.
[16] R. Stoyanova, E. Zhecheva, R. Alcantara, P. Lavela, J.-L. Tirado, Solid State Commun. 102 (1997) 457.
[17] R. Kostecki, F. McLarnon, Electrochem. Solid State Lett. 5 (2002) A164.
[18] D. Ostrovskii, F. Ronci, B. Scrosati, P. Jacobson, J. Power Sources 94 (2001) 183.
[19] D. Aurbach, K. Gamolski, B. Markovsky, G. Salitra, Y. Gofer, U. Heider, R. Oesten, M. Schmidt, J. Electrochem. Soc. 147 (2000) 1322.
[20] K. Dokko, S. Horikoshi, T. Itoh, M. Nishizawa, M. Mohamedi, I. Uchida, J. Power Sources 90 (2000) 109.
[21] E. Zhecheva, R. Stoyanova, Solid State Ionics 66 (1993) 143.
[22] W.W. Huang, R. Frech, Solid State Ionics 86 (8) (1996) 395.
[23] L. Doucey, M. Revault, A. Lautié, A. Chaussé, R. Messina, Electrochim. Acta 44 (1999) 2371.
[24] Zh. Wang, X. Huang, L. Chen, J. Electrochem. Soc. 151 (2004) A1641.